Experimental Applied Mathematics

David H. Bailey and Jonathan M. Borwein

1 Introduction

"Experimental applied mathematics" comprises the usage of modern computer technology as an active agent of research, for the purposes of gaining insight and intuition, discovering new patterns and relationships, testing and conjectures, and confirming analytically derived results, much in the same spirit that laboratory experimentation is employed in the physical sciences. It is closely related to what is known as "experimental mathematics" in pure mathematics, as has been described elsewhere, including the *Princeton Companion* [11].

In one sense, most applied mathematicians have for decades aggressively integrated computer technology into their research. What is meant here is computationally-assisted applied mathematical research that features one or more of the following characteristics:

1. *Computation for exploration and discovery.*
2. *Symbolic computing.*
3. *High-precision arithmetic.*
4. *Integer relation algorithms.*
5. *Graphics and visualization.*
6. *Connections with nontraditional mathematics.*

Depending on the context, the role of rigorous proof in experimental applied mathematics may be much reduced or may be unchanged from that of its pure sister. There are many complex applied problems where there is little point to proving the validity of a minor component rather than finding strong evidence for the appropriateness of the general method.

High-precision arithmetic. Most work in scientific or engineering computing relies on either 32-bit IEEE floating-point arithmetic (roughly seven decimal digit precision) or 64-bit IEEE floating-point arithmetic (roughly 16 decimal digit precision). But for an increasing body of applied mathematical studies, even 16-digit arithmetic is not sufficient. The most common form of high-precision arithmetic is "double-double" or "quad-precision", equivalent to roughly 31-digit precision. Other studies require hundreds or thousands of digits.

Algorithms for performing arithmetic and evaluating common transcendental functions with high-precision data structures have been known for some time, although challenges remain. Mathematical software packages such as *Maple* and *Mathematica* typically include facilities for arbitrarily high precision, but for some applications researchers rely on internet-available software, such as the GNU multiprecision package.

Integer relation detection. Given a vector of real or complex numbers x_i, an *integer relation algorithm* attempts to find a nontrivial set of integers a_i such that $a_1x_1 + a_2x_2 + \cdots + a_nx_n = 0$. One very common application of such an algorithm is to find new identities involving computed numeric constants.

For example, suppose one suspects that an integral (or any other numerical value) x_1 might be a linear sum of a list of terms $x_2, x_3, \cdots, x_n$. One can compute the integral and all the terms to high precision, typically several hundred digits, then provide the vector $(x_1, x_2, \cdots, x_n)$ to an integer relation algorithm. It will either determine that there is an integer-linear relation among these values, or provide a lower bound on the Euclidean norm of any integer relation vector (a_i) that the input vector might satisfy. If the algorithm does produce a relation, then solving it for x_1 produces an experimental identity for the original integral. The most commonly employed integer relation algorithm is the "PSLQ" algorithm of mathematician-sculptor Helaman Ferguson, although the Lenstra-Lenstra-Lovasz (LLL) algorithm can also be adapted for this purpose.

2 Historical examples

The best way to clarify what is meant by experimental applied mathematics is to show some examples of this paradigm in action.

Gravitational boosting. One interesting space-age example is the unexpected discovery of *gravitational boosting* by Michael Minovitch at the Jet Propulsion Laboratory in 1961. Minovitch described how he discovered that *Hohmann transfer ellipses* were not, as then believed, the minimum-energy way to reach the outer planets. Instead, he discovered computationally that spacecraft orbits which pass close by other planets could gain a "slingshot effect" substantial boost in speed (compensated by an extremely small change in the orbital velocity of the planet) on their way to a distant location. Until this demonstration, "most planetary mission designers considered the gravity field of a target planet to be somewhat of a nuisance, to be cancelled out, usually by onboard Rocket thrust."

Without such a boost from Jupiter, Saturn and Uranus, the Voyager mission would have taken more than 30 years to reach Neptune; instead, Voyager reached Neptune in only ten years. Indeed, without gravitational boosting, we would still be waiting! We would have to wait much longer for Voyager to leave the solar system as it now is.

One premier example of 20th century applied experimental mathematics is the development of *fractal theory*, as exemplified by the works of Benoit Mandelbrot. Mandelbrot studied many more examples of fractal sets, many of them with direct connections to nature. Applications include analyses of the shapes of coastlines, mountains, biological structures, blood vessels, galaxies, even music, art and the stock market. For example, Mandelbrot found that the coast of Australia, the West Coast of Britain and the land frontier of Portugal all satisfy shapes given by a fractal dimension of approximately 1.75.

In the 1960s and early 1970s, applied mathematicians began to computationally explore features of chaotic iterations that had previously been studied by analytic methods. May, Lorenz, Mandelbrot, Feigenbaum, Ruelle, York and others led the way in utilizing computers and graphics to explore this realm, as chronicled for example in Gleick's book *Chaos: Making a New Science*.

The uncertainty principle. We finish this section with a principle that, while discovered early in the 20th century by conventional formal reasoning, could have been discovered much more easily with computational tools.

Most readers have heard of the *uncertainty principle* from quantum mechanics, which is often expressed as the fact that the position and momentum of a subatomic-scale particle cannot simultaneously be prescribed or measured to arbitrary accuracy. Others may be familiar with the uncertainty principle from signal processing theory, which is often expressed as the fact that a signal cannot simultaneously be "time-limited" and "frequency-limited." Remarkably, the precise mathematical formulations of these two principles are identical.

Consider a real, continuously differentiable, L^2 function $f(t)$, which further satisfies $|t|^{3/2+\varepsilon} f(t) \to 0$ as $|t| \to \infty$ for some $\varepsilon > 0$. (This assures convergence of the integrals below.) For convenience, we assume $f(-t) = f(t)$, so the Fourier transform $\hat{f}(x)$ of $f(t)$ is real, although this is not necessary. Define

$$E(f) = \int_{-\infty}^{\infty} f^2(t)\,\mathrm{d}t \qquad V(f) = \int_{-\infty}^{\infty} t^2 f^2(t)\,\mathrm{d}t$$
$$\hat{f}(x) = \int_{-\infty}^{\infty} f(t) e^{-itx}\,\mathrm{d}t \quad Q(f) = \frac{V(f)}{E(f)} \cdot \frac{V(\hat{f})}{E(\hat{f})}. \tag{1}$$

Then the uncertainty principle is the assertion that $Q(f) \geq 1/4$, with equality if and only if $f(t) = ae^{-(bt)^2/2}$ for real constants a and b. The proof of this fact is not terribly difficult but is hardly enlightening—see, for example [5, pg. 183–188].

Let us approach this problem as an experimental mathematician might. As mentioned, it is natural when studying Fourier transforms (particularly in the context of signal processing) to consider the "dispersion" of a function and to compare this with the dispersion of its Fourier transform. Noting what appears to be an inverse relationship between these two quantities, we are led to consider $Q(f)$ in (1). With the assistance of *Maple* or *Mathematica*, one can readily work out some examples, as shown in Table 1. Note that each of the entries in the last column is in the range $(1/4, 1/2)$. Can one get any lower?

To further study this problem experimentally, note that the Fourier transform $\hat{f}$ of $f(t)$ can be closely approximated with a *Fast Fourier transform*, after suitable discretization. The integrals

$f(t)$	Interval	$\hat{f}(x)$	$Q(f)$
$1-t\,\mathrm{sgn}\,t$	$[-1,1]$	$2(1-\cos x)/x^2$	$3/10$
$1-t^2$	$[-1,1]$	$4(\sin x - x\cos x)/x^3$	$5/14$
$1/(1+t^2)$	$[-\infty,\infty]$	$\pi\exp(-x\,\mathrm{sgn}\,x)$	$1/2$
$e^{-\lvert t\rvert}$	$[-\infty,\infty]$	$2/(1+x^2)$	$1/2$
$1+\cos t$	$[-\pi,\pi]$	$2\sin(\pi x)/(x-x^3)$	$(\pi^2-15/2)/9$

Table 1: Q values for various functions.

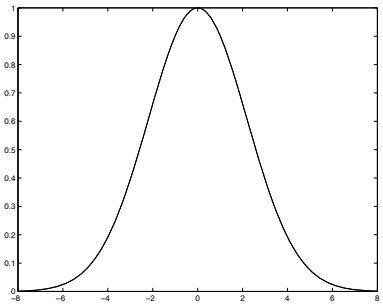

Figure 1: Q-minimizer and matching Gaussian.

V and E can be similarly evaluated numerically. Then one can adopt a search strategy, starting, say, with a "tent function," then perturbing it up or down by some δ on a regular grid. *When for a given δ, a minimizing function $f(t)$ has been found, reduce δ, refine the grid and repeat. Terminate when δ is sufficiently small, say* 10^{-6} *or so.* (For additional details, see [5].)

The resulting function $f(t)$ is shown in Figure 1. Needless to say, its shape strongly suggests a *Gaussian* probability curve. Figure 1 displays both $f(t)$ and the function $e^{-(bt)^2/2}$, where $b = 0.45446177$—they are identical to the precision of the plot!

In short, it is a relatively simple matter, using 21st-century computational tools, to numerically "discover" the uncertainty principle. Doubtless the same is true of many other historical principles of physics, chemistry and other fields.

3 21st century studies

It is fair to say that the computational-experimental approach in applied mathematics has greatly accelerated in the 21st century. We show here a few specific illustrative examples. These include several by the present authors, because we are familiar with them. There are doubtless many others that we are not aware of that are similarly exemplary of the experimental paradigm.

3.1 Chimera states in oscillator arrays

One interesting example of experimental applied mathematics was the 2002 discovery by Kuramoto, Battogtokh and Sima of "chimera" states, which arise in certain nonlocally coupled oscillator systems (i.e., arrays of identical oscillators, where individual oscillators are correlated with oscillators some distance away in the array). These systems can arise in a wide range of physical systems, including Josephson junction arrays, oscillating chemical systems, epidemiological models, neural networks underlying snail shell patterns and "ocular dominance stripes" observed in the visual cortex of cats and monkeys. In chimera states, named for the mythological beast that incongruously combines features of lions, goats and serpents, the oscillator array bifurcates into two relatively stable groups, the first composed of coherent, phased-locked oscillators, and the second composed of incoherent, drifting oscillators.

According to Abrams and Strogatz, who subsequently studied these states in detail, most arrays of oscillators quickly converge into one of four typical patterns: (a) synchrony, with all oscillators moving in unison; (b) solitary waves in one dimension or spiral waves in two dimensions, with all oscillators locked in frequency; (c) incoherence, where phases of the oscillators vary quasi-periodically, with no global spatial structure; and (d) more complex patterns, such as spatiotemporal chaos and intermittency. But in chimera states, phase locking and incoherence are simultaneously present in the same system.

The simplest governing equation for a continuous one-dimensional chimera array is

$$\frac{\partial\phi}{\partial t} = \omega - \int_0^1 G(x-x')\sin\left[\phi(x,t)-\phi(x',t)+\alpha\right]\,\mathrm{d}x', \tag{2}$$

where $\phi(x,t)$ specifies the phase of the oscillator given by $x \in [0,1)$ at time t, and $G(x-x')$ specifies the degree of nonlocal coupling between the oscillators x and x'. A discrete, computable version of (2) can be obtained by replacing the integral with a sum over a 1-D array $(x_k,\, 0 \le k < N)$,

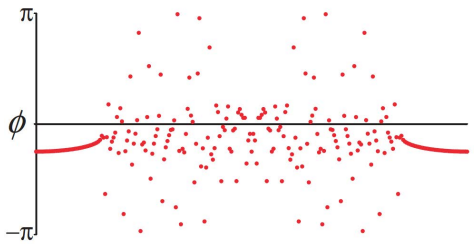

Figure 2: Phase pattern for a typical chimera state.

where $x_k = k/N$. Kuramoto and Battogtokh took $G(x - x') = C\exp(-\kappa|x - x')$ for constant C and parameter κ.

Specifying $\kappa = 4$, $\alpha = 1.457$, array size $N = 256$ and time step size $\Delta t = 0.025$, and starting from $\phi(x) = 6\exp\left[-30(x - 1/2)^2\right] r(x)$, where r is a uniform random variable on $[-1/2, 1/2)$, gives rise to the phase patterns shown in Figure 2. Note that the oscillators near $x = 0$ and $x = 1$ appear to be phase-locked, moving in near-perfect synchrony with their neighbors, but those oscillators in the center drift wildly in phase, both with respect to their neighbors and to the locked oscillators.

Numerous researchers have studied this phenomenon since its initial numerical discovery. Abrams and Strogatz studied the coupling function is given by $G(x) = (1 + A\cos x)/(2\pi)$, where $0 \le A \le 1$, for which they were able to solve the system analytically, and then extended their methods to more general systems. They found that chimera systems have a characteristic life cycle: a uniform phase-locked state, followed by a spatially uniform drift state, then a modulated drift state, then the birth of a chimera state, followed a period of stable chimera, then a saddle-node bifurcation, and finally an unstable chimera.

3.2 Winfree oscillators

One closely related development is the resolution of the Quinn-Rand-Strogatz (QRS) constant. Quinn, Rand and Strogatz had studied the *Winfree model* of coupled nonlinear oscillators, namely

$$\dot{\theta}_i = \omega_i + \frac{\kappa}{N}\sum_{j=1}^{N} -(1 + \cos\theta_j)\sin\theta_i \qquad (3)$$

for $1 \le i \le N$, where $\theta_i(t)$ is the phase of oscillator i at time t, the parameter κ is the coupling strength, and the frequencies ω_i are drawn from a symmetric unimodal density $g(w)$. In their analyses, they were led to the formula

$$0 = \sum_{i=1}^{N}\left(2\sqrt{1 - s^2(1 - 2(i-1)/(N-1))^2} - \frac{1}{\sqrt{1 - s^2(1 - 2(i-1)/(N-1))^2}}\right),$$

implicitly defining a phase offset angle $\phi = \sin^{-1} s$ due to bifurcation. The authors conjectured, on the basis of numerical evidence, the asymptotic behavior of the N-dependent solution s to be

$$1 - s_N \sim \frac{c_1}{N} + \frac{c_2}{N^2} + \frac{c_3}{N^3}\cdots,$$

where $c_1 = 0.60544365\ldots$ is now known as the QRS constant.

In 2008, the present authors together with Richard Crandall computed the numerical value of this constant to 42 decimal digits, obtaining

$$c_1 \approx 0.605443657196732749478922842 44\ldots.$$

With this numerical value in hand, they were able to demonstrate that c_1 is the unique zero of the *Hurwitz zeta* function $\zeta(1/2, z/2)$ on the interval $0 \le z \le 2$. What's more, they found that $c_2 = -0.104685459\ldots$ is given analytically by

$$c_2 = c_1 - c_1^2 - 30\frac{\zeta(-1/2, c_1/2)}{\zeta(3/2, c_1/2)}.$$

3.3 High precision dynamics.

Periodic orbits form the "skeleton" of a dynamical system and provide much useful information, but when the orbits are unstable, high-precision numerical integrators are often required to obtain numerically meaningful results.

For instance, in Figure 3 we show computed symmetric periodic orbit for the (7+2)-Ring problem using double and quadruple precision. The $(n + 2)$-*body Ring problem* describes the motion of an infinitesimal particle attracted by the gravitational field of $n + 1$ primary bodies, n in the vertices of a regular polygon is rotating in its own plane about the center with constant angular velocity. Each point corresponds to the initial conditions of one symmetric periodic orbit, and the grey

area corresponds to regions of forbidden motion (delimited by the limit curve). To avoid "false" initial conditions it is useful to check if the initial conditions generate a periodic orbit up to a given tolerance level; but for highly unstable periodic orbits we may lose several digits in each period, so that double precision is not enough, resulting in gaps in the figure.

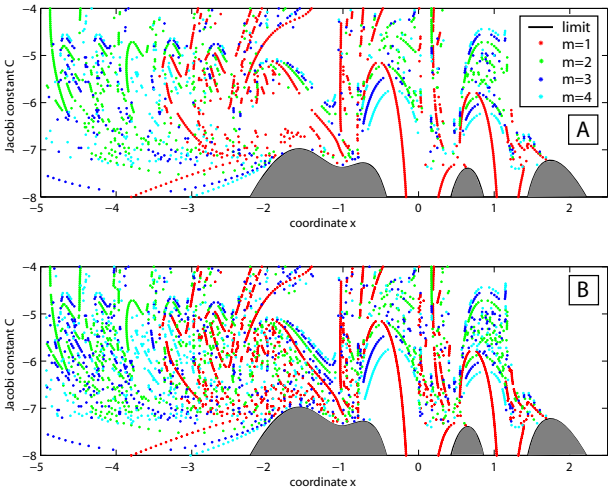

Figure 3: Symmetric periodic orbits (m denotes multiplicity of the periodic orbit) in the most chaotic zone of the (7+2)-Ring problem using double (A) and quadruple (B) precision. (Reproduced by permission.)

Hundred-digit precision arithmetic plays a fundamental role in a 2010 study of the fractal properties of the LORENZ ATTRACTOR [3.XY] (see Figure 4). The first plot shows the intersection of an arbitrary trajectory on the Lorenz attractor with the section $z = 27$, in a rectangle in the $x - y$ plane. All later plots zoom in on a tiny region (too small to be seen by the unaided eye) at the center of the red rectangle of the preceding plot to show that what appears to be a line is in fact not one.

The Lindstedt-Poincaré method for computing periodic orbits is based on the Lindstedt-Poincaré perturbation theory, Newton's method for solving nonlinear systems, and Fourier interpolation. Viswanath has used this in combination with high-precision libraries to obtain periodic orbits for the Lorenz model at the classical Saltzman's parameter values. This procedure permits one to compute, to high accuracy, highly unstable periodic orbits that otherwise would lose all numerical significance. For these reasons, high-precision arithmetic plays a fundamental role in the study of the fractal properties of the Lorenz attractor (see Figures 4 and 5) and in a consistent formal development of complex singularities of the Lorenz system using infinite series.

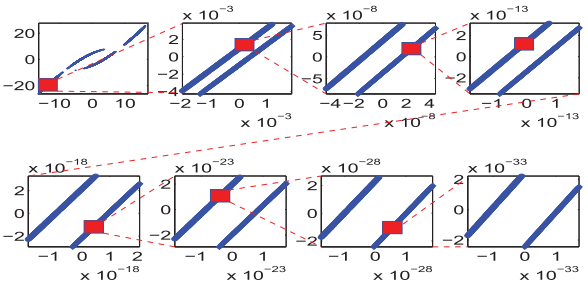

Figure 4: Fractal property of the Lorenz attractor. (Reproduced by permission.)

For additional details and references, see [4].

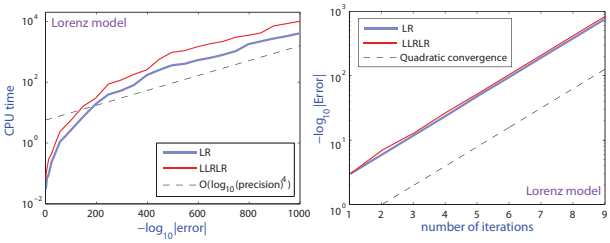

Figure 5: Computational relative error vs. CPU time and number of iterations in a 1000-digit computation of the periodic orbits LR and LLRLR of the Lorenz model. (Reproduced by permission.)

3.4 Ising integrals

The previously mentioned study employed 100-digit arithmetic. Much higher precision has proven essential in studies with Richard Crandall (see [5, 2]) of the following integrals that arise in the Ising theory of mathematical physics and in quan-

tum field theory:

$$C_n = \frac{4}{n!}\int_0^\infty \cdots \int_0^\infty \frac{1}{\left(\sum_{j=1}^n (u_j + 1/u_j)\right)^2}\,\mathrm{d}U$$

$$D_n = \frac{4}{n!}\int_0^\infty \cdots \int_0^\infty \frac{\prod_{i<j}\left(\frac{u_i-u_j}{u_i+u_j}\right)^2}{\left(\sum_{j=1}^n (u_j + 1/u_j)\right)^2}\mathrm{d}U$$

$$E_n = 2\int_0^1 \cdots \int_0^1 \left(\prod_{1\le j<k\le n} \frac{u_k - u_j}{u_k + u_j}\right)^2 \mathrm{d}T,$$

where $\mathrm{d}U = \frac{\mathrm{d}u_1}{u_1}\cdots\frac{\mathrm{d}u_n}{u_n}$, $\mathrm{d}T = \mathrm{d}t_2\cdots\mathrm{d}t_n$, and $u_k = \prod_{i=1}^k t_i$. Note that $E_n \le D_n \le C_n$.

Direct computation of these integrals from their defining formulas is very difficult, but for C_n, it can be shown that

$$C_n = \frac{2^n}{n!}\int_0^\infty pK_0^n(p)\,\mathrm{d}p,$$

where K_0 is the *modified Bessel function*. Numerical values so computed were used with PSLQ to deduce results such as $C_4 = 7\zeta(3)/12$, and furthermore to discover that

$$\lim_{n\to\infty} C_n = 0.63047350\ldots \;=\; 2e^{-2\gamma},$$

with additional higher-order terms in an asymptotic expansion. One intriguing experimental result (not yet proven) is the following:

$$\begin{aligned} E_5 \stackrel{?}{=}\; & 42 - 1984\,\mathrm{Li}_4\left(\frac{1}{2}\right) + \frac{189\pi^4}{10} - 74\zeta(3) \\ & - 1272\zeta(3)\log 2 + 40\pi^2\log^2 2 - \frac{62\pi^2}{3} \\ & + \frac{40\pi^2\log 2}{3} + 88\log^4 2 + 464\log^2 2 - 40\log 2, \end{aligned}$$

found by a multi-hour computation on a highly parallel computer system, and confirmed to 250-digit precision. Here $\mathrm{Li}_4(z) = \sum_{k\ge1} z^k/k^4$ is the standard order-4 polylogarithm.

3.5 Ramble integrals and short walks

Consider, for complex s, the n-dimensional *ramble integrals* [3]

$$W_n(s) = \int_{[0,1]^n} \left|\sum_{k=1}^n e^{2\pi x_k i}\right|^s \mathrm{d}x, \qquad (4)$$

which occur in the theory of uniform random walk integrals in the plane, where at each step a unit-step is taken in a random direction as first studied by Pearson, Rayleigh and others a hundred years ago. Integrals such as (4) are the s-th moment of the distance to the origin after n steps. As is well known, various types of random walks arise in fields as diverse as aviation, ecology, economics, psychology, computer science, physics, chemistry, and biology.

Walks and measures. In 2010 work (by J. Borwein, A. Straub , J. Wan and W. Zudilin), using a combination of analysis and high-precision numerical computation, results such as

$$W_n'(0) = -n\int_0^\infty \log(x)J_0^{n-1}(x)J_1(x)\mathrm{d}x,$$

were obtained, where $J_n(x)$ denotes the Bessel function of the first kind and γ denotes Euler's constant. These results, in turn, lead to various closed forms and have been used to confirm, to 600-digit precision, the following *Mahler measure* conjecture adapted from Villegas:

$$\begin{aligned} W_5^{'}(0) \stackrel{?}{=} \left(\frac{15}{4\pi^2}\right)^{5/2}\int_0^\infty \big\{ & \eta^3(e^{-3t})\eta^3(e^{-5t}) \\ & + \eta^3(e^{-t})\eta^3(e^{-15t})\big\}\, t^3\,\mathrm{d}t, \end{aligned}$$

where the *Dedekind eta-function* can be computed from: $\eta(q) =$

$$q^{1/24}\prod_{n\ge1}(1-q^n) = q^{1/24}\sum_{n=-\infty}^{\infty}(-1)^n q^{n(3n+1)/2}.$$

There are remarkable connections between diverse parts of pure, applied and computational mathematics lying behind these results. As often there is a fine interplay between developing better computational tools—especially for special functions and polylogarithms—and discovering new structure.

Densities of short walks. One of the deepest related discoveries is the following closed form for the *radial density* of a four step uniform random walk in the plane: for $2 \le \alpha \le 4$ one has the real hypergeometric form:

$$p_4(\alpha) = \frac{2}{\pi^2}\frac{\sqrt{16-\alpha^2}}{\alpha}\,{}_3F_2\left(\left.\begin{matrix}\frac{1}{2},\frac{1}{2},\frac{1}{2}\\ \frac{5}{6},\frac{7}{6}\end{matrix}\right| \frac{\left(16-\alpha^2\right)^3}{108\alpha^4}\right).$$

Remarkably the real part of the right side of this identity is valid everywhere on $[0, 4]$, as plotted in Figure 6. This was an entirely experimental

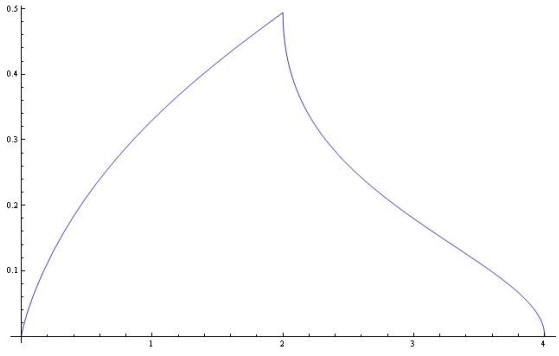

Figure 6: The "shark-fin" density of a four step walk.

discovery—involving at least one fortunate error—but is now fully proven.

3.6 Moments of elliptic integrals

The previous study on ramble integrals also led to a comprehensive analysis of moments of elliptic integral functions of the form:

$$\int_0^1 x^{n_0} K^{n_1}(x) K'^{n_2}(x) E^{n_3}(x) E'^{n_4}(x) \mathrm{d}x,$$

where the elliptic functions K, E and their complementary versions are:

$$K(x) = \int_0^1 \frac{\mathrm{d}t}{\sqrt{(1-t^2)(1-x^2t^2)}}$$
$$E(x) = \int_0^1 \frac{\sqrt{1-x^2t^2}}{\sqrt{1-t^2}}\,\mathrm{d}t$$
$$K'(x) = K(\sqrt{1-x^2}) \qquad E'(x) = E(\sqrt{1-x^2}).$$

Computations of these integrals to 3200-digit precision, combined with searches for relations using the PSLQ algorithm, yielded thousands of unexpected relations among these integrals (see [3]). The scale of the computation was required by the number of integrals under investigation.

3.7 Snow crystals

Computational experimentation has even been useful in the study of snowflakes. In a 2007 study, Janko Gravner and David Griffeath used a sophisticated computer-based simulator to study the process of formation of these structures, known in the literature as snow crystals and informally as *snofakes*. Their model simulated each of the key steps, including diffusion, freezing, and attachment, and thus enabled researchers to study, dependence on melting parameters. Snow crystals produced by their simulator vary from simple stars, to six-sided crystals with plate-ends, to crystals with dendritic ends, and look remarkably similar to natural snow crystals. Among the findings uncovered by their simulator is the fact that these crystals exhibit remarkable overall symmetry, even in the process of dynamically changing parameters. Their simulator is publicly available at `http://psoup.math.wisc.edu/Snofakes.htm`.

4 Limits of computation

Developments such as the above have led to re-examination of the role of computation in formal mathematical work. To begin with, a legitimate question is whether one can truly trust—in the mathematical sense—the result of a computation, since there are many possible sources of errors: unreliable numerical algorithms; bug-ridden computer programs implementing these algorithms; system software or compiler errors; hardware errors, either in processing or storage; insufficient numerical precision; and obscure errors of hardware, software or programming that surface only in particularly large or difficult computations.

As a single example of the sorts of difficulties that can arise, the present authors found that neither *Maple* nor *Mathematica* was able to numerically evaluate constants of the form

$$\frac{1}{2\pi}\int_0^{2\pi} f(e^{i\theta})\,\mathrm{d}\theta$$

where $f(\theta) = \mathrm{Li}_1(\theta)^m \mathrm{Li}_1^{(1)}(\theta)^p \mathrm{Li}_1(\theta+\pi)^n \mathrm{Li}_1^{(1)}(\theta-\pi)^q$ (for $m, n, p, q \geq 0$ integers) to high precision in reasonable run time. In part this was because of the challenge of computing polylog and polylog derivatives (with respect to order) at complex arguments. The version of *Mathematica* that we were using was able to numerically compute $\partial \mathrm{Li}_s(z)/\partial s$ to high precision, which is required here, but such evaluations were not only

many times slower than $\mathrm{Li}_s(z)$ itself, but in some cases did not even return a tenth of the requested number of digits correctly.

For such reasons, experienced programmers of mathematical or scientific computations routinely insert validity checks in their code. Typically such checks take advantage of known high-level mathematical facts, such as the fact that the product of two matrices used in the calculation should always give the identity, or that the results of a convolution of integer data, done using a fast Fourier transform, should all be very close to integers.

For instance, Kanada's 2002 computation of π to 1.3 trillion decimal digits involved first computing slightly over one trillion hexadecimal (base-16) digits. He found that the 20 hex digits of π beginning at position $10^{12}+1$ are `B4466E8D21 5388C4E014`. Kanada then calculated these hex digits using the "Bailey-Borwein-Plouffe" algorithm. The result was `B4466E8D21 5388C4E014`, dramatically confirming that both results are almost certainly correct. While one cannot rigorously assign a "probability" to this event, the chances that two random strings of 20 hex digits perfectly agree is one in $16^{20} \approx 1.2089 \times 10^{24}$.

Even so, researchers are well-advised to be cautious with experimentation. Consider:

$$\int_0^\infty \cos(2x) \prod_{n=1}^{\infty} \cos(x/n)\,\mathrm{d}x \tag{5}$$
$$= 0.392699081698724154807830422909937860524645\underline{4341872315959}26\ldots.$$

At first glance, this appears to be $\pi/8$, but upon comparison with the numerical value

$$\pi/8 = 0.392699081698724154807830422909937860524646\underline{1749218882276}21\ldots,$$

the two values disagree after the 42nd digit!

Richard Crandall later explained this mystery, via a physically motivated analysis of *running out of fuel* random walks. He found the following very rapidly convergent series expansion, of which formula (5) is the first term:

$$\frac{\pi}{8} = \sum_{m=0}^{\infty} \int_0^\infty \cos[2(2m+1)x] \prod_{n=1}^{\infty} \cos(x/n)\,\mathrm{d}x.$$

Two series terms suffice for 500-digit agreement.

As a final sobering example, consider

$$\sigma_p = \sum_{n=-\infty}^{\infty} \mathrm{sinc}(n/2)\,\mathrm{sinc}(n/3)\cdots\mathrm{sinc}(n/p)\,\mathrm{d}x$$
$$\stackrel{?}{=} \int_{-\infty}^{\infty} \mathrm{sinc}(x/2)\,\mathrm{sinc}(x/3)\cdots\mathrm{sinc}(x/p)\,\mathrm{d}x,$$

where the denominators range over *all* primes up to p. Provably, the following is true: The "sum equals integral" identity for σ_p remains valid at least for p among roughly the first 10^{176} primes; but stops holding after some larger prime, and thereafter the "sum less the integral" is strictly positive, but *they always differ by much less than one part in a googolplex* $= 10^{10^{100}}$. An even stronger estimate is possible assuming the Generalized Riemann Hypothesis.

Further Reading

1. D.M. Abrams and S.H. Strogatz, "Chimera states in a ring of nonlocally coupled oscillators," *Intl. J. of Bifur. and Chaos*, vol. 16 (2006), 21–37.
2. D.H. Bailey and J.M. Borwein, "Exploratory experimentation and computation," *Notices of the AMS*, vol. 58 (Nov 2011), 1410–19.
3. D.H. Bailey and J.M. Borwein, "Hand-to-hand combat with thousand-digit integrals," *J. Comp. Science*, vol. 3 (2012), 77–86.
4. D.H. Bailey, R. Barrio and J.M. Borwein, "High-precision computation: Mathematical physics and dynamics," *Appl. Math. and Comp.*, vol. 218 (2012), 10106–10121.
5. J.M. Borwein and D.H. Bailey, *Mathematics by Experiment: Plausible Reasoning in the 21st Century*, AK Peters, 2008.
6. J.M. Borwein and K. Devlin, *The Computer as Crucible: an Introduction to Experimental Mathematics*, AK Peters, 2008.
7. J. Gleick, *Chaos: The Making of a New Science*, Viking Penguin, New York, 1987.
8. J. Gravner and D. Griffeath, "Modeling snow crystal growth: A three-dimensional mesoscopic approach," *Phys. Rev. E*, vol. 79 (2009), 011601.
9. B.B. Mandelbrot, *The Fractal Geometry of Nature*, W. H. Freeman, New York, 1982.
10. M. Minovitch, "A method for determining interplanetary free-fall reconnaissance trajectories," *JPL Tech. Memo TM-312-130*, 38–44 (8.23.1961).
11. H.S. Wilf, "Mathematics: An experimental science," *The Princeton Companion to Mathematics*, Princeton University Press, 2008.
12. S. Wolfram, *A New Kind of Science*, Wolfram Media, Champaign, IL, 2002.